

Coordination for Connected Automated Vehicles at Merging Roadways in Mixed Traffic Environment

Viet-Anh Le, *Student Member, IEEE*, Hao M. Wang, Gábor Orosz, *Senior Member, IEEE*,
and Andreas A. Malikopoulos, *Senior Member, IEEE*

Abstract—In this paper, we present a two-level optimal control framework to address motion coordination of connected automated vehicles (CAVs) in the presence of human-driven vehicles (HDVs) in merging scenarios. Our framework combines an unconstrained trajectory solution of a low-level energy-optimal control problem with an upper-level optimization problem that yields the minimum travel time for CAVs. We predict the future trajectories of the HDVs using Newell’s car-following model. To handle potential deviations of HDVs’ actual behavior from the one predicted, we provide a risk-triggered re-planning mechanism for the CAVs based on time-to-conflict. The effectiveness of the proposed control framework is demonstrated via simulations with heterogeneous human driving behaviors and via experiments in a scaled environment.

I. INTRODUCTION

Emerging vehicular technologies in automation and communication have generated new opportunities to enhance traffic safety and efficiency [1]. Prior research efforts have shown that in environments consisting solely of connected automated vehicles (CAVs), the traffic throughput and energy consumption can be significantly improved under different vehicle coordination strategies such as optimal control [2], [3], virtual platooning [4], model predictive control [5], and learning-based control [6]. It is expected that CAVs will gradually penetrate the market and interact with human-driven vehicles (HDVs) over the next several years. The presence of HDVs, however, complicates vehicle coordination, given the existing limitations on predicting precise driving behavior.

Addressing coordination of CAVs in a mixed-traffic environment, where CAVs and HDVs co-exist, has attracted considerable attention recently. Game theory combined with reinforcement learning has been used to model human decision-making and determine an optimal action sequence for intelligent agents in [7]. Mixed-integer linear programming for centralized scheduling and coordinating CAVs interacting with HDVs was proposed in [8]. Other approaches include dynamic programming [9], statistical modeling of human uncertainties [10], and reachability analysis [11].

This work was supported by NSF under Grants CNS-2149520 and CMMI-2219761.

Viet-Anh Le and Andreas A. Malikopoulos are with the Department of Mechanical Engineering, University of Delaware, Newark, DE 19716 USA (emails: {vietale, andreas}@udel.edu.)

Hao M. Wang and Gábor Orosz are with the Department of Mechanical Engineering, University of Michigan, Ann Arbor, MI 48109, USA. {haowangm, orosz}@umich.edu.

Gábor Orosz is also with the Department of Civil and Environmental Engineering, University of Michigan, Ann Arbor, MI 48109, USA.

In mixed autonomy, traffic bottlenecks such as merging roadways and intersections pose significant challenges to the decision-making and control of CAVs. A multi-agent reinforcement learning framework for CAVs was presented in [12] for microscopic simulation where the human drivers are simulated by a car-following model. A hierarchical on-ramp merging control strategy for CAVs was presented in [13], where an upper-level planner computes an expected merging position and a low-level trajectory controller guarantees constraints under uncertainties of HDVs. The problem of vehicle platoon formation in a mixed traffic environment by only controlling the CAVs and then coordinating the platoons led by CAVs was addressed in [14]. A vehicle coordination problem for a signal-free intersection using vehicle platooning was addressed in [15], where each platoon is formed by a leading CAV, multiple trailing HDVs, and a tail CAV. Wang et al. [16] presented a conflict analysis framework to resolve conflicts between vehicles of different automation levels. The available information was summarized by means of conflict charts, which enable fast and reliable decision-making and controller design.

In this paper, we extend the framework developed in [2], [17] for CAV coordination in a mixed-traffic merging scenario. We present an optimal control formulation to derive the trajectories for the CAVs, in which the unconstrained solution of a low-level energy-optimal control problem is embedded in the upper-level optimization problem aimed to ensure the minimum travel time for the CAV. We employ Newell’s car-following model [18] to predict the HDVs’ future trajectories, which are used to formulate no-conflict constraints in the optimal control problem. The latter helps each CAV avoid conflicts with the vehicles traveling on the same road and those traveling on the other merging road. Since the predicted trajectories may deviate from those arising from the human drivers’ actions, we perform a risk-triggered re-planning based on the time-to-conflict [19]. Once time-to-conflict is smaller than a given threshold, we re-solve the optimal control problem to derive a new trajectory for the CAV. We demonstrate the efficacy of the proposed framework by simulations given different levels of CAV penetration and traffic volumes and by experiments with scaled robotic vehicles.

The remainder of the paper proceeds as follows. In Section II, we formulate the coordination problem of CAVs in a mixed-traffic merging scenario. In Section III, we present the optimal control problem formulation combined with a method for predicting the future trajectories of HDVs

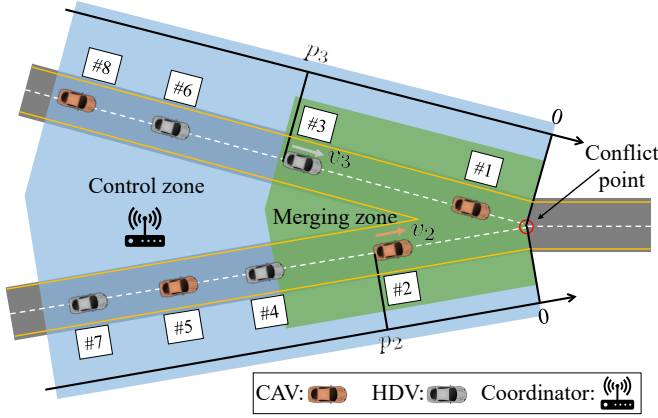


Fig. 1: Merge scenario with two merging roadways intersecting at a conflict point. The control zone is represented by the blue area. In the merging zone (green area) virtual projection is utilized as detailed in Section III-B.

and a risk-triggered re-planning mechanism. We provide simulation results in Section IV, and experimental validation in Section V. Finally, we draw concluding remarks in Section VI.

II. PROBLEM FORMULATION

We consider the problem of coordinating multiple CAVs, co-existing with HDVs, in a highway merging scenario, where two merging roadways intersect at a position called conflict point, i.e., the point where the two roadways merge (Fig. 1). We consider that a *coordinator* is available who has access to the motion information of all vehicles (including CAVs and HDVs). In our framework, we define a control zone inside of which the CAVs exchange information with each other and the coordinator. Communication errors or delays are neglected. The analysis of such effects is left for future research.

Next, we provide the following necessary definitions for our exposition.

Definition 1: Let $\mathcal{L}(t) = \{1, \dots, L(t)\}$, $t \in \mathbb{R}_{\geq 0}$, be the set of vehicles traveling inside the control zone, where $L(t) \in \mathbb{N}$ is the total number of vehicles. Let $\mathcal{A}(t) \subset \mathcal{L}(t)$ and $\mathcal{H}(t) \subset \mathcal{L}(t)$ be the sets of CAVs and HDVs, respectively. For example, considering the scenario in Fig. 1, $\mathcal{L}(t) = \{1, \dots, 8\}$, $\mathcal{A}(t) = \{1, 2, 5, 8\}$, and $\mathcal{H}(t) = \{3, 4, 6, 7\}$. Note that the indices of the vehicles are determined by the order they enter the control zone.

Definition 2: For a vehicle $i \in \mathcal{L}(t)$, let $\mathcal{R}_{i,S}(t) \subset \mathcal{L}(t)$ and $\mathcal{R}_{i,N}(t) \subset \mathcal{L}(t)$, $t \in \mathbb{R}_{\geq 0}$, be the sets of vehicles inside the control zone traveling on the same road as vehicle i and on the neighboring road, respectively.

We consider that the dynamics of each vehicle $i \in \mathcal{L}(t)$ are described by a double integrator model:

$$\begin{aligned} \dot{p}_i(t) &= v_i(t), \\ \dot{v}_i(t) &= u_i(t), \end{aligned} \quad (1)$$

where $p_i \in \mathcal{P}$, $v_i \in \mathcal{V}$, and $u_i \in \mathcal{U}$ denote the longitudinal position of the rear bumper, speed, and control input (acceleration/deceleration) of the vehicle, respectively. The sets \mathcal{P} , \mathcal{V} , and \mathcal{U} are compact subsets of \mathbb{R} . Note that we set

$p_i = 0$ at the conflict point; see Fig. 1. The control input is bounded by

$$u_{\min} \leq u_i(t) \leq u_{\max}, \quad \forall i \in \mathcal{L}(t), \quad (2)$$

where $u_{\min} < 0$ and $u_{\max} > 0$ are the minimum and maximum control inputs as designated by the physical acceleration and braking limits of the vehicles, or limits that can be imposed for driver/passenger comfort. Next, we provide the speed limits of the CAVs,

$$v_{\min} \leq v_i(t) \leq v_{\max}, \quad \forall i \in \mathcal{A}(t), \quad (3)$$

where $v_{\min} = 0$ and $v_{\max} > 0$ are the minimum and maximum allowable speeds. Note that we do not impose speed limits for HDVs since they can be violated by human driving behavior. However, we assume that the speed of HDVs is lower bounded by 0, i.e., $v_i(t) \geq 0$, $\forall i \in \mathcal{H}(t)$, which means the HDVs do not go backward.

To avoid conflicts between vehicles, we impose two types of constraints: (i) between the vehicles traveling on different roads (to avoid vehicles meeting at the conflict point); and (ii) between the vehicles traveling on the same road (to avoid rear-end collisions). To prevent a potential conflict between CAV- i and a vehicle $k \in \mathcal{R}_{i,N}(t)$ traveling on the neighboring road, we require a minimum time gap $t_{\min} > 0$ between the time instants t_i^f and t_k^f when the CAV- i and vehicle k cross the conflict point, i.e.,

$$|t_i^f - t_k^f| \geq t_{\min}. \quad (4)$$

To prevent rear-end collision between CAV- i and its immediate preceding vehicle k traveling on the same road, where $k = \max\{j \in \mathcal{R}_{i,S}(t) \mid j < i\}$, we impose the following rear-end safety constraint:

$$p_k(t) - p_i(t) \geq d_{\min} + t_h v_i(t), \quad (5)$$

where $d_{\min} > 0$ and $t_h > 0$ are the minimum distance at a standstill and safe time headway. Note that here we use the distance between the vehicles' rear bumpers, and the vehicle length is included by choosing sufficiently large d_{\min} in (5).

III. OPTIMAL CONTROL FORMULATION

In this section, we present an optimal control framework to coordinate the CAVs in mixed traffic. This framework extends the one we developed in [2], [17] for 100% CAV penetration. For each CAV- i , we use the unconstrained trajectory solution of a low-level energy-minimal optimal control problem to formulate the upper-level optimization problem that obtains the minimum time required to cross the conflict point, i.e., t_i^f , while satisfying all state, control, and safety constraints.

A. Optimal Control Problems

We start our exposition with the low-level optimization by considering that the solution to the upper-level optimization problem is known, i.e., we consider the minimum time t_i^f that satisfies all constraints has been determined. Given t_i^f , the low-level optimal control problem aims at finding the optimal

control input (acceleration/deceleration) for each CAV by solving the following problem.

Problem 1: (Low-level energy-optimal control) Let t_i^0 and t_i^f be the times that CAV- i enters and exits the control zone, respectively. Then, CAV- i solves the following optimal control problem at t_i^0 :

$$\begin{aligned} & \underset{u_i(t) \in \mathcal{U}}{\text{minimize}} && \frac{1}{2} \int_{t_i^0}^{t_i^f} u_i^2(t) dt, \\ & \text{subject to:} && \\ & && (1), (2), (3), \\ & && (5), k = \max \{j \in \mathcal{R}_{i,S}(t_i^0) \mid j < i\}, \end{aligned} \quad (6)$$

given:

$$p_i(t_i^0) = p^0, v_i(t_i^0) = v_i^0, p_i(t_i^f) = 0, u_i(t_i^f) = 0,$$

where p^0 is the position of the control zone at the entry point. The boundary conditions in (6) are set at the entry and exit of the control zone.

Note that (4) is not included in the low-level problem. The reason is that time t_i^f derived by the upper-level problem, discussed next, satisfies (4). Note that in (6) we minimize the L^2 norm of control input $u_i(t)$ in $t \in [t_i^0, t_i^f]$. However, the actual energy consumption per unit mass for a vehicle is

$$\varepsilon = \int_{t_i^0}^{t_i^f} v_i(t)g(u_i(t)) dt, \quad (7)$$

where $g(x) = \max\{0, x\}$. It was shown in [20], [21] that the energy consumption (7) can be upper and lower bounded by the cost function in (6). Therefore, minimizing the L^2 norm of the control input (acceleration/deceleration) can benefit energy efficiency.

The closed-form solution of Problem 2 for each CAV- i can be derived using the Hamiltonian analysis [2]. In case that none of the state and control constraints are active, the unconstrained Hamiltonian is formulated as

$$H_i(t, p_i(t), v_i(t), u_i(t)) = \frac{1}{2} u_i^2(t) + \lambda_i^p v_i(t) + \lambda_i^v u_i(t), \quad (8)$$

where λ_i^p and λ_i^v are co-states corresponding to position and speed, respectively. The Euler-Lagrange equations of optimality are given by

$$\dot{\lambda}_i^p = -\frac{\partial H_i}{\partial p_i} = 0, \quad (9)$$

$$\dot{\lambda}_i^v = -\frac{\partial H_i}{\partial v_i} = -\lambda_i^p, \quad (10)$$

$$\frac{\partial H_i}{\partial u_i} = u_i + \lambda_i^v = 0. \quad (11)$$

Since the speed of CAV- i is not specified at the travel time t_i^f , we have the boundary condition

$$\lambda_i^v(t_i^f) = 0. \quad (12)$$

Applying the Euler-Lagrange optimality conditions (9)-(11) to the Hamiltonian (8), we obtain the optimal control law

$$u_i^*(t) = -\lambda_i^{v*} = 6a_i t + 2b_i, \quad (13)$$

where a_i and b_i are constants of integration. Therefore, the unconstrained solution takes form

$$\begin{aligned} v_i^*(t) &= 3a_i t^2 + 2b_i t + c_i, \\ p_i^*(t) &= a_i t^3 + b_i t^2 + c_i t + d_i, \end{aligned} \quad (14)$$

where $c_i, d_i \in \mathbb{R}$ are constants of integration. Note that the terminal condition, $u_i(t_i^f) = 0$, results from substituting (12) into (11) at t_i^f , i.e., $u_i(t_i^f) + \lambda_i^v(t_i^f) = 0$. Given the boundary conditions in (6), if t_i^f is known, the constants of integration can be found:

$$\begin{bmatrix} a_i \\ b_i \\ c_i \\ d_i \end{bmatrix} = \begin{bmatrix} (t_i^0)^3 & (t_i^0)^2 & t_i^0 & 1 \\ 3(t_i^0)^2 & 2t_i^0 & 1 & 0 \\ (t_i^f)^3 & (t_i^f)^2 & t_i^f & 1 \\ 6t_i^0 & 2 & 0 & 0 \end{bmatrix}^{-1} \begin{bmatrix} p^0 \\ v_i^0 \\ 0 \\ 0 \end{bmatrix}. \quad (15)$$

Next, we formulate the upper-level optimal control problem to minimize the travel time and guarantee all the constraints for CAVs given the energy-optimal trajectory (14). We enforce this unconstrained trajectory as a motion primitive to avoid real-time implementation and avoid the complexity of solving a constrained optimal control problem by piecing constrained and unconstrained arcs together [22].

Problem 2: (Upper-level minimal-time planning) Once entering the control zone, CAV- i solves the following optimal control problem at t_i^0

$$\begin{aligned} & \underset{t_i^f \in \mathcal{T}_i(t_i^0)}{\text{minimize}} && t_i^f \\ & \text{subject to:} && \\ & && (2), (3), \\ & && (4), \forall k \in \mathcal{R}_{i,N}(t_i^0), \\ & && (5), k = \max \{j \in \mathcal{R}_{i,S}(t_i^0) \mid j < i\}, \\ & && (14), \end{aligned} \quad (16)$$

given:

$$p_i(t_i^0) = p^0, v_i(t_i^0) = v_i^0, p_i(t_i^f) = 0, u_i(t_i^f) = 0.$$

Here the compact set $\mathcal{T}_i(t_i^0) = [t_i^f, \bar{t}_i^f]$ denotes the feasible range of travel time under the state and input constraints of CAV- i computed at t_i^0 .

The computation steps (for more details see [17]) in numerically solving Problem 2 are summarized next: First, we initialize $t_i^f = \bar{t}_i^f$, and compute the parameters $[a_i, b_i, c_i, d_i]$ using (15). We evaluate all the state, control, and no-conflict constraints. If none of the constraints is violated, we return the solution; otherwise, t_i^f is increased by a step size. The procedure is repeated until the solution satisfies all the constraints. By solving Problem 2, the optimal exit time t_i^f along with the optimal trajectory (14) and control law (13) are obtained for CAV- i for $t \in [t_i^0, t_i^f]$.

If a feasible solution to Problem 2 exists, then the solution is a cubic polynomial that guarantees none of the constraints are activated. In case that the solution of Problem 2 does not exist, we can derive an alternative trajectory for the CAVs by solving a two-level optimization problem numerically that includes piecing together the constrained and unconstrained arcs until the solution does not violate any constraints [22].

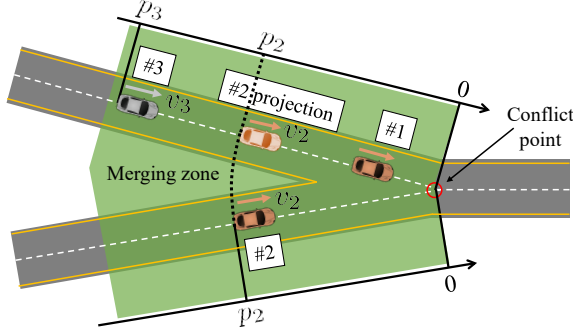


Fig. 2: Virtual projection in the merging zone, where the CAV-2 is projected from the perspective of HDV-3.

B. Human Drivers' Trajectory Prediction

To solve Problem 2 for CAV- i , the trajectories and exit times of all vehicles having potential conflicts with CAV- i must be available. At the time when CAV- i enters the control zone, the trajectories and exit times of other CAVs traveling in the control zone can be obtained from the coordinator via wireless communication. While the state of the HDVs is also assumed to be available, their future trajectories are not known.

Next, we present an approach to predict the future trajectories and exit times of the HDVs traveling in the control zone based on Newell's car-following model [18]. This model simply considers that the position of each vehicle is shifted in time and space from its preceding vehicle's trajectory due to the effect of traffic wave propagation. Specifically, the position of each HDV- k , $k \in \mathcal{H}(t)$, is predicted from the position of its preceding vehicle j as

$$p_k(t) = p_j(t - \tau_k) - w\tau_k, \quad (17)$$

where $\tau_k > 0$ is the time shift of HDV- k , and $w > 0$ is the speed of the backward propagating traffic waves, which is considered to be constant [23]. In this paper, the wave speed is chosen as $w = 5$ m/s.

Since $v_j(t) \geq 0$ and $w > 0$, $p_j(t - \tau_k) - w\tau_k$ is a strictly decreasing function of τ_k . Thus, there exists a unique value of τ_k such that (17) is satisfied for any t . That is, when CAV- i enters the conflict zone at $t = t_i^0$, it can solve (17) for τ_k for each HDV- k based on the positions of the vehicles (obtained from the coordinator). If there is no preceding vehicle in front of HDV- k , it is assumed to maintain its current speed, making its position an affine function of time.

In the proximity of the conflict point, defined as the merging zone in Fig. 1, the HDVs additionally interact with vehicles on the neighboring road to make their decisions. To consider such interactions, we consider the virtual projection of the vehicles to the other road, an example of which is shown in Fig. 2. From the perspective of HDV-3, where the projected CAV-2, instead of CAV-1, is considered as the preceding vehicle. Similar generalized car-following models for merging and lane-changing scenarios have been reported in [4], [24], [25].

Using the proposed prediction model, the position of each HDV in the control zone can be represented by a cubic

polynomial or by an affine function of time. The trajectory prediction is then used for estimating the HDVs' exit times to impose the no-conflict (4) and rear-end safety constraints (5). We use t_k^f and $[a_k, b_k, c_k, d_k]$, $k \in \mathcal{H}(t)$, to denote the predicted exit time and the constants parameterizing the predicted trajectory of HDV- k . Substituting the solution (14) into (17) (for both p_k and p_j), the trajectory parameters of HDV- k can be obtained from those of the preceding vehicle j according to

$$\begin{aligned} a_k &= a_j, \\ b_k &= b_j - 3a_j\tau_k, \\ c_k &= c_j + 3a_j\tau_k^2 - 2b_j\tau_k, \\ d_k &= d_j - a_j\tau_k^3 + b_j\tau_k^2 - c_j\tau_k - w\tau_k, \end{aligned} \quad (18)$$

and t_k^f can be found by solving

$$a_k(t_k^f)^3 + b_k(t_k^f)^2 + c_k t_k^f + d_k = 0. \quad (19)$$

Then t_k^f and $[a_k, b_k, c_k, d_k]$ can be integrated into the constraints (4) and (5) between CAV- i and HDV- k .

C. Risk-Triggered Re-planning

Using Newell's car-following model, we can predict the HDVs' future trajectories and then integrate them into Problem 2 to derive the trajectory and control law for CAVs in the control zone. However, in reality, HDVs may behave differently from the predicted model. Under this discrepancy, the derived optimal control law for CAVs may not always ensure conflict-free maneuvers. To address this issue, we present a risk-triggered re-planning mechanism based on time-to-conflict [19].

To quantify the risk of collision between the CAV- i and its preceding vehicle k , we define the time-to-conflict for rear-end safety (on the same road) as

$$T_i^S(t) = \frac{p_k(t) - p_i(t) - d_{\min}}{v_i(t) - v_k(t)}, \quad (20)$$

for $v_i(t) - v_k(t) > 0$. This indicates the time needed to reach the minimum distance, given the current vehicle positions and speeds. Likewise, we define the time-to-conflict for vehicles traveling on neighboring roads in the merging zone as the time gap between the vehicles crossing the conflict point given their current positions and speeds

$$T_i^N(t) = \left| \frac{-p_i(t) - d_{\min}}{v_i(t)} - \frac{-p_k(t) - d_{\min}}{v_k(t)} \right|, \quad (21)$$

where the minimum distance d_{\min} is included for conservativeness.

If at any time t the control input for CAV- i yields either $T_i^S(t) < T_{cr}^S$ or $T_i^N(t) < T_{cr}^N$, we perform a re-planning, i.e., we find new optimal control law by re-solving Problem 2 given the most recent data as initial conditions. Here T_{cr}^S and T_{cr}^N are the critical time-to-conflict values. Moreover, to improve efficiency, we re-plan if the current vehicle speed is smaller than a pre-defined value \check{v} .

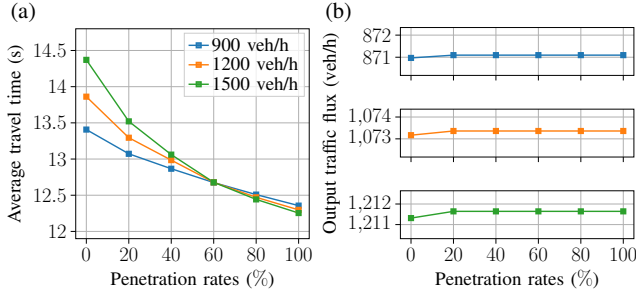


Fig. 3: Average travel time (a) and output traffic flux (b) under different penetration rates of coordinated CAVs.

IV. SIMULATION RESULTS

In this section, we demonstrate the proposed framework by numerical simulations under various penetration rates of CAVs and various traffic volumes.

We consider a merging scenario for a control zone of length 300 m and we define a merging zone of length 75 m upstream of the conflict point. Vehicles enter the control zone with uniformly randomized initial speeds between 22 and 24 m/s. We generate random entering time for the vehicles by a normal distribution where the mean is determined by the traffic volumes. To simulate human-driven vehicles, we utilize the intelligent driver model (IDM) and also consider the virtual projection of the vehicles within the merging zone as shown in Fig. 2; see also [24].

Given a preceding vehicle j (which may be projected from the neighbouring road), the following HDV- k 's control input is given by

$$u_k = a \left(1 - \left(\frac{v_k}{\bar{v}} \right)^4 - \left(\frac{\underline{d} + v_k T - \frac{v_k(v_j - v_k)}{2\sqrt{ab}}}{p_j - p_k} \right)^2 \right), \quad (22)$$

where \bar{v} is the desired speed, \underline{d} is the desired stopping distance, T is the desired time gap, a is the maximum acceleration, and b is the comfortable deceleration. We consider different IDM parameters for different HDVs which are chosen by up to 30% perturbation from the following values: $\bar{v} = 23$ m/s, $\underline{d} = 10$ m, $T = 2$ s, $a = 1$ m/s², $b = 1.5$ m/s². The other parameters used in the controller are $v_{\max} = 25$ m/s, $u_{\min} = -3$ m/s², $u_{\max} = 2$ m/s², $t_{\min} = 2$ s, $d_{\min} = 10$ m, $t_h = 1$ s, $T_{\text{cr}}^S = 3$ s, $T_{\text{cr}}^N = 2$ s, $\bar{v} = 12.5$ m/s.

We conduct simulations using the proposed framework for six CAV penetration rates: 0%, 20%, 40%, 60%, 80%, 100%, and three traffic volumes: 900, 1200, and 1500 vehicles per hour. To quantify the benefits of coordinated CAVs, we use two metrics: average travel time in the control zone of the vehicles and the output traffic flux of the vehicles exiting the control zone. We conduct the simulations with 1000 vehicles to compute those two metrics. Fig. 3 summarizes the results of average travel time and output flux for different CAV penetration rates and traffic volumes. Observe that increasing CAV penetration rate, the average travel time improves significantly. Under high traffic volume (1500 veh/h),

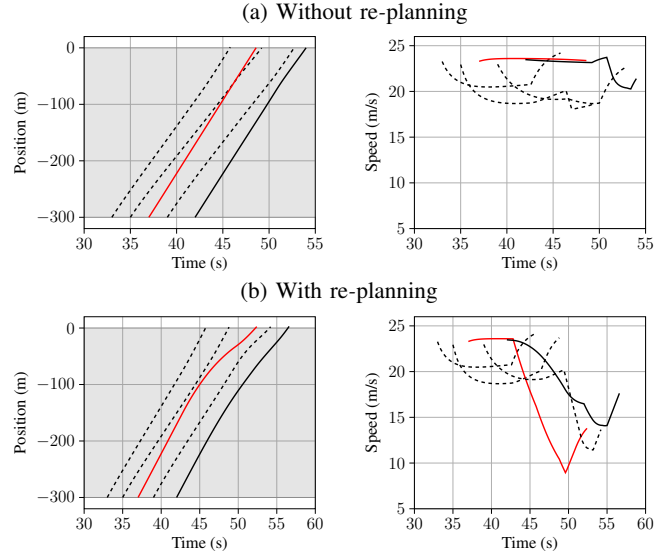


Fig. 4: Simulated position and speed profiles for a CAV and surrounding HDVs without and with risk-triggered re-planning. The trajectories for CAVs and HDVs are represented by red and black curves, respectively. The vehicles moving on different roads are distinguished by solid curves and dashed curves. The gray shaded area highlights the control zone.



Fig. 5: A merge scenario with a conflict point (marked by the red circle) in the Information and Decision Science's Scaled Smart City (IDS³C) [26] used for experimental validation with five vehicles (three CAVs and two HDVs). The black vehicles represent HDVs, while the other vehicles represent CAVs.

100% coordinated CAVs can improve the average travel time by 14% compared to the baseline traffic with pure HDVs. Meanwhile, the differences in the output flux between different levels of CAV penetration are not significant.

To illustrate the risk-triggered re-planning mechanism, the position trajectories and speed profiles of five vehicles, including one CAV and four HDVs, are shown in Fig. 4 for high traffic volume (1500 veh/h). Panel (a) reveals that without re-planning, the optimal trajectory for CAVs derived at the entry of the control zone may cause an unsafe situation since the prediction from Newell's car-following model is inaccurate, whereas if re-planning is activated, we can derive a new trajectory so that the CAV can avoid a collision (Fig. 4b).

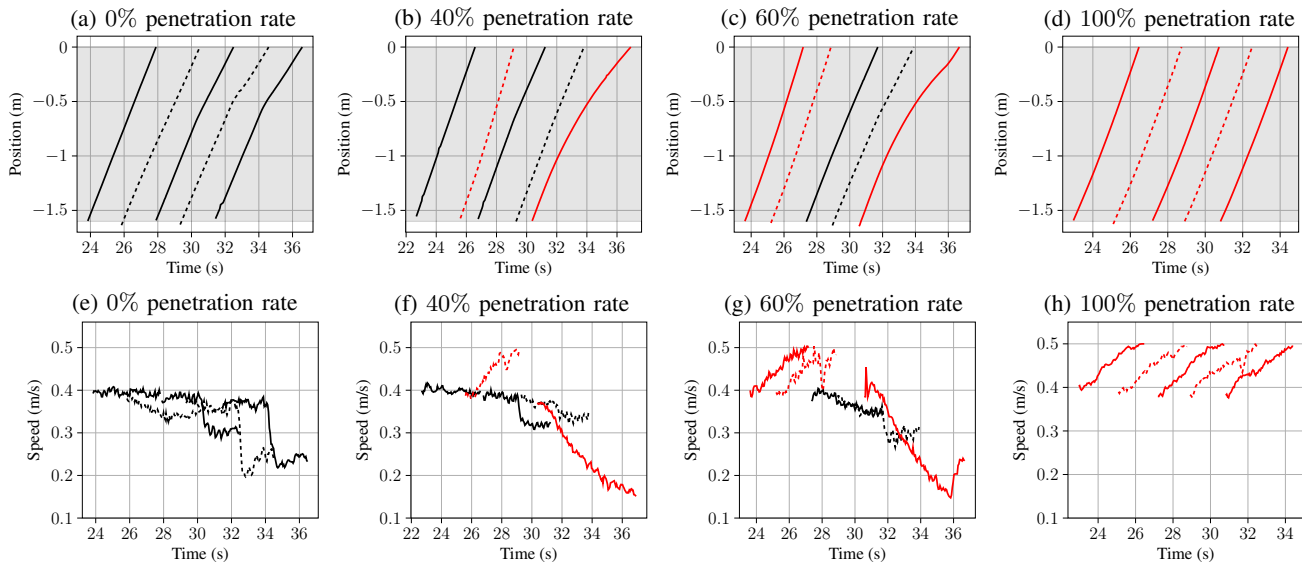


Fig. 6: Position and speed profiles of five vehicles in experiments. The trajectories for CAVs and HDVs are represented by red and black curves, respectively. The vehicles moving on different roads are distinguished by solid curves and dashed curves. The gray region highlights the control zone.

V. EXPERIMENTAL DEMONSTRATION

To validate the real-time practicality of our presented framework, we perform experiments of a merging scenario in a scaled robotic testbed called Information and Decision Science’s Scaled Smart City (IDS³C) [26]. The vehicle positions are obtained from a VICON motion capture system, while the speeds are computed from the difference equation combined with a low-pass filter for noise cancellation. A multithreaded C++ program running on a mainframe computer with a 3 GHz Intel Core i7-6950X CPU and 128 GB is considered as the coordinator. The coordinator collects the localization data from the VICON system, computes the desired trajectory, and transmits it to the vehicles via UDP/IP protocol. The computation and communication between the mainframe and the vehicles happen at every 50 ms, i.e., the frequency is 20 Hz. Note that the presented framework results in light computation to implement the controller in real-time at the rate of 20 Hz. The robotic vehicles equipped with Raspberry Pi 3B embedded computers receive trajectory information from the mainframe and then use a modified Stanley controller for lane tracking and a PID controller to track the desired speed profile. We use five scaled robotic vehicles for CAVs and HDVs in the experiments and consider a merging problem with a control zone of length 1.6 m and a merging zone of length 1.0 m. The experimental setup is shown in Fig. 5. Similar to the simulation setup, we employ IDM with virtual projection to replicate human drivers. In the experiment, we used the following parameters: $v_{\max} = 0.5$ m/s, $u_{\min} = -0.5$ m/s², $u_{\max} = 0.5$ m/s², $t_{\min} = 2.0$ s, $t_h = 1.2$ s, $d_{\min} = 0.25$ m, $T_{\text{cr}}^{\text{S}} = 2.0$ s, $T_{\text{cr}}^{\text{N}} = 1.5$ s, $\tilde{v} = 0.15$ m/s.

The longitudinal position trajectories and speed profiles of five vehicles in the control zone are depicted in Fig. 6 for four

experiments with different penetration rates of CAVs. As can be seen from the figures, the CAVs could cross the merging zone with safe distances and time gaps with the HDVs. Under partial penetration, since CAVs and HDVs behave conservatively, the traffic is slowed down, while under full penetration, the experiment witnessed the full elimination of stop-and-go driving. If re-planning is not activated, the speed profiles of the CAVs roughly follow the quadratic energy-optimal form (14), whereas the speed profiles for HDVs generated by IDM with virtual projection cause abrupt deceleration when the vehicles approach the conflict point.

Videos of the experiments and other results can be found on the following website <https://sites.google.com/view/ud-ids-lab/CAV-HDV>.

VI. CONCLUSION

In this paper, we extended the coordination framework developed in prior work [2] for CAVs in mixed traffic on-ramp merging. We presented a two-level optimal control formulation, where the low-level optimization minimizes the CAVs’ energy consumption while the upper-level optimization minimizes the CAVs’ travel time. We utilized Newell’s car-following model with virtual projection to predict human driving behavior, and a risk-triggered re-planning algorithm was used to address possible unsafe situations. The simulation and experimental results demonstrated the performance and implications of the framework. Future research should enhance this framework to address multiple lanes and conduct extensive studies in a mixed traffic environment under different penetration rates of CAVs.

REFERENCES

- [1] T. Eرسال, I. Kolmanovsky, N. Masoud, N. Ozay, J. Scruggs, R. Vasudevan, and G. Orosz, “Connected and automated road vehicles: state of

- the art and future challenges,” *Vehicle System Dynamics*, vol. 58, no. 5, pp. 672–704, May 2020.
- [2] A. A. Malikopoulos, L. E. Beaver, and I. V. Chremos, “Optimal time trajectory and coordination for connected and automated vehicles,” *Automatica*, vol. 125, no. 109469, 2021.
 - [3] J. I. Ge and G. Orosz, “Optimal control of connected vehicle systems with communication delay and driver reaction time,” *IEEE Transactions on Intelligent Transportation Systems*, vol. 18, no. 8, pp. 2056–2070, 2017.
 - [4] A. I. M. Medina, N. van de Wouw, and H. Nijmeijer, “Automation of a T-intersection using virtual platoons of cooperative autonomous vehicles,” in *18th International Conference on Intelligent Transportation Systems*, 2015, pp. 1696–1701.
 - [5] A. Katriniok, B. Rosarius, and P. Mähönen, “Fully distributed model predictive control of connected automated vehicles in intersections: Theory and vehicle experiments,” *IEEE Transactions on Intelligent Transportation Systems*, vol. 23, no. 10, pp. 18 288–18 300, 2022.
 - [6] B. Chalaki, L. E. Beaver, B. Remer, K. Jang, E. Vinitsky, A. Bayen, and A. A. Malikopoulos, “Zero-shot autonomous vehicle policy transfer: From simulation to real-world via adversarial learning,” in *IEEE 16th International Conference on Control & Automation (ICCA)*, 2020, pp. 35–40.
 - [7] B. M. Albaba and Y. Yildiz, “Modeling cyber-physical human systems via an interplay between reinforcement learning and game theory,” *Annual Reviews in Control*, vol. 48, pp. 1–21, 2019.
 - [8] S. Ravikumar, R. Quirynen, A. Bhagat, E. Zeino, and S. Di Cairano, “Mixed-integer Programming for Centralized Coordination of Connected and Automated Vehicles in Dynamic Environment,” in *2021 IEEE Conference on Control Technology and Applications (CCTA)*. IEEE, 2021, pp. 814–819.
 - [9] M. Karimi, C. Roncoli, C. Alecsandru, and M. Papageorgiou, “Cooperative merging control via trajectory optimization in mixed vehicular traffic,” *Transportation Research Part C: Emerging Technologies*, vol. 116, p. 102663, 2020.
 - [10] A. Bajcsy, S. L. Herbert, D. Fridovich-Keil, J. F. Fisac, S. Deglurkar, A. Dragan, and C. Tomlin, “A scalable framework for real-time multi-robot, multi-human collision avoidance,” *International Conference on Robotics and Automation (ICRA)*, pp. 936–943, 2019.
 - [11] M. Koschi and M. Althoff, “Set-based prediction of traffic participants considering occlusions and traffic rules,” *IEEE Transactions on Intelligent Vehicles*, vol. 6, no. 2, pp. 249–265, 2021.
 - [12] Z. Yan and C. Wu, “Reinforcement learning for mixed autonomy intersections,” in *IEEE International Intelligent Transportation Systems Conference (ITSC)*. IEEE, 2021, pp. 2089–2094.
 - [13] H. Liu, W. Zhuang, G. Yin, Z. Li, and D. Cao, “Safety-critical and flexible cooperative on-ramp merging control of connected and automated vehicles in mixed traffic,” *IEEE Transactions on Intelligent Transportation Systems*, 2023.
 - [14] A. M. I. Mahhub and A. A. Malikopoulos, “A Platoon Formation Framework in a Mixed Traffic Environment,” *IEEE Control Systems Letters (LCSS)*, vol. 6, pp. 1370–1375, 2021.
 - [15] M. Faris, P. Falcone, and J. Sjöberg, “Optimization-based coordination of mixed traffic at unsignalized intersections based on platooning strategy,” in *IEEE Intelligent Vehicles Symposium (IV)*. IEEE, 2022, pp. 977–983.
 - [16] H. M. Wang, S. S. Avedisov, T. G. Molnár, A. H. Sakr, O. Altintas, and G. Orosz, “Conflict analysis for cooperative maneuvering with status and intent sharing via V2X communication,” *IEEE Transactions on Intelligent Vehicles*, vol. 8, no. 2, pp. 1105–1118, 2023.
 - [17] B. Chalaki, L. E. Beaver, and A. A. Malikopoulos, “Experimental validation of a real-time optimal controller for coordination of cavs in a multi-lane roundabout,” in *IEEE Intelligent Vehicles Symposium (IV)*, 2020, pp. 504–509.
 - [18] G. F. Newell, “A simplified car-following theory: a lower order model,” *Transportation Research Part B: Methodological*, vol. 36, no. 3, pp. 195–205, 2002.
 - [19] S. S. Avedisov, G. Bansal, and G. Orosz, “Impacts of connected automated vehicles on freeway traffic patterns at different penetration levels,” *IEEE Transactions on Intelligent Transportation Systems*, vol. 23, no. 5, pp. 4305–4318, 2022.
 - [20] C. R. He, J. I. Ge, and G. Orosz, “Fuel efficient connected cruise control for heavy-duty trucks in real traffic,” *IEEE Transactions on Control Systems Technology*, vol. 28, no. 6, pp. 2474–2481, 2020.
 - [21] M. Shen, C. R. He, T. G. Molnar, A. H. Bell, and G. Orosz, “Energy-efficient connected cruise control with lean penetration of connected vehicles,” *IEEE Transactions on Intelligent Transportation Systems*, pp. 1–13, 2023.
 - [22] A. A. Malikopoulos, C. G. Cassandras, and Y. J. Zhang, “A decentralized energy-optimal control framework for connected automated vehicles at signal-free intersections,” *Automatica*, vol. 93, pp. 244–256, 2018.
 - [23] T. G. Molnár, X. A. Ji, S. Oh, D. Takács, M. Hopka, D. Upadhyay, M. Van Nieuwstadt, and G. Orosz, “On-board traffic prediction for connected vehicles: implementation and experiments on highways,” in *American Control Conference (ACC)*. IEEE, 2022, pp. 1036–1041.
 - [24] K. Kreutz and J. Eggert, “Analysis of the generalized intelligent driver model (GIDM) for merging situations,” in *IEEE Intelligent Vehicles Symposium (IV)*. IEEE, 2021, pp. 34–41.
 - [25] Y. Guo, Q. Sun, R. Fu, and C. Wang, “Improved car-following strategy based on merging behavior prediction of adjacent vehicle from naturalistic driving data,” *IEEE Access*, vol. 7, pp. 44 258–44 268, 2019.
 - [26] B. Chalaki, L. E. Beaver, A. M. I. Mahhub, H. Bang, and A. A. Malikopoulos, “A research and educational robotic testbed for real-time control of emerging mobility systems: From theory to scaled experiments,” *IEEE Control Systems*, vol. 42, no. 6, pp. 20–34, 2022.